Generic optical singularities and beam-field phenomena due to general paraxial beam reflection at a plane dielectric interface

Anirban Debnath ●* and Nirmal K. Viswanathan ●†

School of Physics, University of Hyderabad, Hyderabad 500046, India

A single paraxial beam reflection at a plane dielectric interface, configured appropriately, can lead to the formation of a polarization singularity in the inhomogeneously polarized output beam field for any central angle of incidence. In this paper we derive the necessary condition to realize this effect. We explore the phase singularity characteristics associated with this polarization-singular field and explore the dynamics of the singularities due to controlled variations of the input polarization. The simulation-generated exact field information lead to the exploration of the unique Goos-Hänchen, Imbert-Fedorov, and spin shifts of the optical-singular fields and the anticipation of an exact mathematical characterization of spin-orbit interaction phenomena involved therein. The formation of a phase singularity independent of a polarization singularity is explained subsequently. Interrelating these seemingly unconnected beam-field phenomena and generic optical singularities can lead to a significant and fundamental understanding of the inhomogeneously polarized beam field; additionally, our singularity generation method can find potential application in experimental characterization of the involved dielectric media.

I. INTRODUCTION

The reflection and transmission of an ideal plane electromagnetic wave at a plane isotropic dielectric interface is one of the fundamental problems in electromagnetic optics [1]. However, an ideal plane wave does not physically exist; instead, a real optical beam can be decomposed into constituent ideal plane waves, each of which can be analyzed individually to understand their reflection and transmission. The composite output beams thus generated exhibit fundamentally significant beam-field phenomena—such as Goos-Hänchen (GH) shift, Imbert-Fedorov (IF) shift, and longitudinal and transverse spin shifts—decades of extensive studies on which are present in the literature [2–27].

A different class of special characteristics of beam fields are the phase and polarization singularities [28]. A phase singularity is a point in the beam field where the phase of the field is indeterminate. This occurs when both the real and the imaginary parts of the field are zero [28–35]. A *C*-point polarization singularity in the beam field is a point where the orientation of the polarization ellipse is undefined (but handedness is defined) [28,33,34,36–47]. A point containing either a $\hat{\sigma}^+$ or a $\hat{\sigma}^-$ spin polarization, and surrounded by other polarizations (usually arranged in the beam field in special patterns such as lemon, star and monstar), is a *C*-singularity point.

The formation of phase singularities due to Brewster reflection was first identified by Barczyk *et al.* [48]; and subsequently, in Refs. [49] and [50], we have examined the formation and transitional dynamics of generic polarization

singularities in a Brewster-reflected paraxial beam field. In the present paper, we show that the above Brewster-reflection effects constitute a subset of a larger class of phenomena that occur due to any general central angle of incidence. If an optical system is configured to give, e.g., a $\hat{\sigma}^-$ spin-polarized reflected beam in the ideal case for any given angle of incidence, the wavefront curvature of the real beam causes the appearance of the intended $\hat{\sigma}^-$ polarization only at the beam center and noncircular (approximately $\hat{\sigma}^-$) polarizations in the surrounding region. This causes the appearance of a *C*-point polarization singularity at the beam center. By appropriately configuring the input polarization, the above scheme can be generalized to create a polarization singularity anywhere in the beam field. We derive the necessary condition to generate such a singularity in the beam field for a general angle of incidence and show that the above-mentioned Brewster-reflection effects [48–50] can be seamlessly derived as a special case of the obtained condition. Additionally, we interpret the $\hat{\sigma}^-$-polarized *C* singularity as an attribution of an associated phase-singular $\hat{\sigma}^+$-polarized field, and subsequently demonstrate the dynamics of these phase and polarization singularities due to controlled variations in the optical system. The present paper thus provides a fundamental and significant understanding of the existence of phase and polarization singularities in a general reflected paraxial beam field for any given central angle of incidence.

Even though we use a Fresnel-coefficient-based calculation only at the central plane of incidence to explain the concerned optical singularity formations, we obtain the simulated field profiles by using our generalized reflection and transmission coefficient matrix formalism [51], via which the exact field information of the final output beam is available. As explained in Ref. [51], the various novel beam-field properties and phenomena such as GH and IF shifts, spin shifts,

---

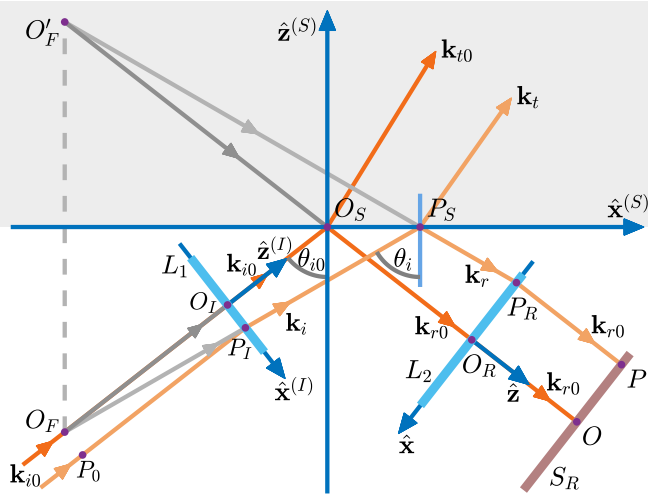*anirban.debnath090@gmail.com
†nirmalsp@uohyd.ac.in

FIG. 1. The simulated optical system to analyze the reflection of a paraxially diverging optical beam.

geometric phase characteristics [52–58]—and spin-orbit interaction (SOI) phenomena in general [15,16,19,56–61]—are different manifestations of the same fundamental inhomogeneously polarized nature of the beam field; and all these phenomena are exactly characterizable by using the available complete field information. By using the computationally generated exact field information, we demonstrate the GH, IF, and spin shift phenomena in the context of the presently considered optical-singular fields, and explore their unique variations due to the variation of the optical system configuration. We then propose that the exact field information can lead to a complete mathematical characterization of the SOI characteristics of the beam field, which are anticipated to be significant and fundamentally interesting, especially in the context of the presently considered optical-singular fields. Subsequently, we explain how a phase-singular field can be achieved independent of a polarization singularity, leading to a special decomposition of an inhomogeneously polarized field as a superposition of a dominant plane-wave or near-plane-wave field and a remnant orthogonally polarized phase-singular field. Such a special decomposition is anticipated to have strong interrelation to the special beam-field phenomena. To summarize, the special beam-field phenomena studied in the current literature and the optical-singular phenomena discussed in the present paper are all manifestations of the same fundamental polarization inhomogeneity of the beam field; and hence all these phenomena are interrelated. We explore some of these interrelations in the present paper; and further interrelations, including a detailed mathematical characterization of SOI phenomena of the present optical-singular fields, are to be explored in the future. In addition, our singularity formation method is anticipated to have potential application in experimental measurements of refractive indices of dielectric media.

II. THE OPTICAL SYSTEM AND FIELD TRANSFORMATION

We simulate an optical system (Fig. 1) based on the one we have used in Ref. [51] (the same coordinate system

conventions are implied). In this system, an initial collimated Gaussian beam is diverged through a lens L_1 (focal length $\mathcal{F}_1 < 0$). The resulting spherically diverging paraxial beam is incident at a plane isotropic dielectric interface with a central angle of incidence θ_{i0}. The refractive indices of the incidence and transmission media are respectively n_1 and n_2. The reflected spherically diverging paraxial beam propagates to a lens L_2 (focal length $\mathcal{F}_2 > 0$) which collimates the beam. Finally, the beam profile is observed at the screen S_R. As shown in Fig. 1, O_F is the focus of L_1 ($\mathcal{F}_1 = -O_F O_I$), and O'_F is the image of O_F (the beam field never truly exists in these regions; so we validly consider O_F and O'_F as point sources of the incident and reflected diverging beams respectively for the purpose of the geometrical analysis). So the distances $O_I O_S$ and $O_S O_R$ are adjusted to get $O_F O_I + O_I O_S + O_S O_R = \mathcal{F}_2$, ensuring the final collimation.

We need to consider only the central plane of incidence ($y^{(I)} = y^{(S)} = y = 0$) for the present paper. In this plane, we consider an arbitrary ray path $P_0 \rightarrow P_I \rightarrow P_S \rightarrow P_R \rightarrow P$ (Fig. 1), along which a set of constituent wavefront surface elements are considered to propagate. If the $x^{(I)}$ coordinate of P_I is x_I, then the x coordinate of P_R is obtained by the system geometry as $x_R = -\alpha x_I$, where $\alpha = \mathcal{F}_2/|\mathcal{F}_1|$. The same geometry also shows that, as an associated spherical surface element propagates from P_I to P_R, its area expands by a factor α^2, due to the inverse square law.

We now consider an input surface-element field at P_0 as (suppressing the $\mathbf{k} \cdot \mathbf{r} - \omega t$ phase term)

$$\boldsymbol{\mathcal{E}}_0^{(I)} = \mathcal{E}_{0x}^{(I)} \hat{\mathbf{x}}^{(I)} + e^{i\Phi_E} \mathcal{E}_{0y}^{(I)} \hat{\mathbf{y}}^{(I)}, \tag{1a}$$

$$\mathcal{E}_{0x}^{(I)} = \mathcal{E}_{00} \, G_I \cos\theta_E, \quad \mathcal{E}_{0y}^{(I)} = \mathcal{E}_{00} \, G_I \sin\theta_E, \tag{1b}$$

where $\mathcal{E}_{00}$ represents the central field magnitude; $G_I = e^{-x_I^2/w_0^2}$ represents the Gaussian distribution along the $x^{(I)}$ axis with a half-width w_0; and (θ_E, Φ_E) represent the angle and relative-phase parameters determining the field polarization. As this element field propagates to P, it is (1) unaltered along $P_0 \rightarrow P_I$ and $P_R \rightarrow P$; (2) modified by the lenses L_1 and L_2 at P_I and P_R respectively; (3) reduced in amplitude by a factor $g = 1/\alpha$ due to the surface-element area expansion along $P_I \rightarrow P_S \rightarrow P_R$; and (4) modified by Fresnel reflection coefficients at P_S. We have analytically verified that, at the central plane of incidence, the modifications due to L_1 and L_2 exactly compensate for each other; and hence, their exact analysis is not required here.

At the central plane of incidence, the $\hat{\mathbf{x}}^{(I)}$ and $\hat{\mathbf{y}}^{(I)}$ components of $\boldsymbol{\mathcal{E}}_0^{(I)}$ [Eq. (1a)] are respectively the transverse magnetic (TM) and transverse electric (TE) components. Hence, at P_S these components acquire Fresnel TM and TE reflection coefficients $r_{\mathrm{TM}}(\theta_i)$ and $r_{\mathrm{TE}}(\theta_i)$ respectively [1], where, θ_i is the angle of incidence at P_S. The final output field at P is thus obtained as

$$\boldsymbol{\mathcal{E}} = \mathcal{E}_x \hat{\mathbf{x}} + e^{i\Phi_E} \mathcal{E}_y \hat{\mathbf{y}}, \tag{2a}$$

$$\mathcal{E}_x = \mathcal{E}_R \, r_{\mathrm{TM}}(\theta_i) \cos\theta_E, \quad \mathcal{E}_y = \mathcal{E}_R \, r_{\mathrm{TE}}(\theta_i) \sin\theta_E, \tag{2b}$$

$$\mathcal{E}_R = g \, \mathcal{E}_{00} \, G_R, \quad G_I \equiv G_R = e^{-x_R^2/w_R^2}, \quad w_R = \alpha \, w_0. \tag{2c}$$

Since the ray path $P_0 \rightarrow P$ is arbitrary, the field $\boldsymbol{\mathcal{E}}$ [Eq. (2a)] truly represents the final output electric field as a function of

$x \equiv x_R$ at the linear section of the screen S_R at the central plane of incidence.

III. POLARIZATION SINGULARITY FORMATION

A. Generalized condition

As understood from Eq. (2b), the Gaussian function G_R is modified by $r_{\mathrm{TM}}(\theta_i)$ and $r_{\mathrm{TE}}(\theta_i)$ respectively to generate different field functions $\mathcal{E}_x(x)$ and $\mathcal{E}_y(x)$. However, for a given specific point $x = x_S$ in the beam field, it is possible to find a specific value $\theta_E = \theta_{ES}$ that satisfies

$$|\tan\theta_{ES}| = |r_{\mathrm{TM}}(\theta_i)/r_{\mathrm{TE}}(\theta_i)|_{x=x_S}, \tag{3}$$

resulting in $|\mathcal{E}_x| = |\mathcal{E}_y|$ only at $x = x_S$. Under this condition, either a $\hat{\boldsymbol{\sigma}}^+$ or a $\hat{\boldsymbol{\sigma}}^-$ spin polarization can be generated at $x = x_S$ by choosing $\Phi_E = \pm\pi/2$ in Eq. (2a). Equation (2b) ensures that another $\hat{\boldsymbol{\sigma}}^{\pm}$ polarization does not appear in the immediate vicinity of $x = x_S$, since $|\mathcal{E}_x| = |\mathcal{E}_y|$ is not satisfied at other points in the immediate vicinity.

While the condition of Eq. (3) is written based on the field functions at the x axis only [Eq. (2b)], we have computationally verified based on the formalism of Ref. [51] that no other immediately neighboring point at the screen S_R (xy plane) in general contains a $\hat{\boldsymbol{\sigma}}^{\pm}$ polarization under the above condition. An isolated $\hat{\boldsymbol{\sigma}}^{\pm}$ polarization, i.e., a C-point singularity, is thus obtained at the specific point $x = x_S$.

Thus, summarizing the central result of the present paper, a polarization singularity is obtained at a point $P(x_S, 0)$ at the screen S_R, for any central angle of incidence θ_{i0}, if the initial input polarization parameter values (θ_E, Φ_E) are chosen as (θ_{ES}, Φ_{ES}), where

$$\tan\theta_{ES} = \pm\left|\frac{r_{\mathrm{TM}}(\theta_i)}{r_{\mathrm{TE}}(\theta_i)}\right|_{x=x_S}, \qquad \Phi_{ES} = \pm\frac{\pi}{2}. \tag{4}$$

This result reveals the significant fact that, when configured appropriately, even one simple reflection of a paraxial Gaussian beam at a plane dielectric interface, for any angle of incidence, can generate a polarization singularity in the reflected beam field.

B. Functional variation of θ_{ES}

For the purpose of simulations and experimental results in the present paper, it is convenient to show the formation of a polarization singularity at the central-ray point O ($x_S = 0$) at the screen S_R (Fig. 1). For $x_S = 0$, Eq. (4) gives

$$\tan\theta_{ES} = \pm\left|\frac{r_{\mathrm{TM}}(\theta_{i0})}{r_{\mathrm{TE}}(\theta_{i0})}\right| = \pm\left|\frac{\cos(\theta_{i0}+\theta_{t0})}{\cos(\theta_{i0}-\theta_{t0})}\right|, \tag{5a}$$

$$\theta_{t0} = \sin^{-1}\left[(n_1/n_2)\sin\theta_{i0}\right] \quad \text{(Snell's law)}, \tag{5b}$$

obtained using the Fresnel coefficient expressions [1] ($c_i = \cos\theta_{i0}$, $c_t = \cos\theta_{t0}$)

$$r_{\mathrm{TM}}(\theta_{i0}) = (n_2 c_i - n_1 c_t)/(n_2 c_i + n_1 c_t), \tag{6a}$$

$$r_{\mathrm{TE}}(\theta_{i0}) = (n_1 c_i - n_2 c_t)/(n_1 c_i + n_2 c_t). \tag{6b}$$

The variation of θ_{ES} as a function of θ_{i0} [Eq. (5a)], for $n_1 = 1$ and $n_2 = 1.52$, is shown in Fig. 2. Some of the notable characteristics of this variation are as follows:
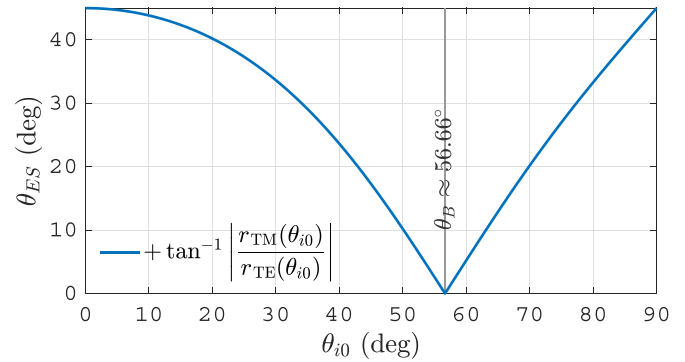

FIG. 2. Variation of θ_{ES} as a function of θ_{i0} [Eq. (5a)], considering the singularity generation at the reflected beam center. The plot shows only the positive solution $\theta_{ES} = +\tan^{-1}|r_{\mathrm{TM}}(\theta_{i0})/r_{\mathrm{TE}}(\theta_{i0})|$ for convenience; both $\pm\tan^{-1}|r_{\mathrm{TM}}(\theta_{i0})/r_{\mathrm{TE}}(\theta_{i0})|$ are valid solutions.

(1) For $\theta_{i0} = 0°$, we have $|r_{\mathrm{TM}}(0°)| = |r_{\mathrm{TE}}(0°)| = (n_2 - n_1)/(n_2 + n_1)$. So, to satisfy the condition of Eq. (5a), we have $\theta_{ES} = \pm45°$.

(2) For $\theta_{i0} \to 90°$, we have $r_{\mathrm{TM}}(\theta_{i0}) \approx r_{\mathrm{TE}}(\theta_{i0}) \to -1$. Hence, we have $\theta_{ES} \to \pm45°$ to satisfy the condition of Eq. (5a).

(3) For Brewster angle incidence $\theta_{i0} = \theta_B = \tan^{-1}(n_2/n_1)$, we have $r_{\mathrm{TM}}(\theta_B) = 0$. Thus, to satisfy Eq. (5a), we must have $\theta_{ES} = 0°$. This is the only special case where, according to Eq. (2b), both $\mathcal{E}_x$ and $\mathcal{E}_y$ must become zero at O to create a singularity. It is thus a higher-order V-point singularity (both handedness and orientation are undefined [47]) but not a simple C-point singularity. The formation of this V-point singularity, however, can be explained in terms of a merger of two C-point singularities, as we have explained in our earlier work [50].

Figure 2 clearly shows that the formation of a polarization singularity due to Brewster reflection is seamlessly identified by considering $\theta_{i0} = \theta_B$ in the general condition of Eq. (5a), which is a remarkable result, since this generalization has not been anticipated in previous works [48–50]. Our entire work of Ref. [50] can thus be considered as a special-case analysis of the present work on generalized singularity generation due to paraxial beam reflection.

IV. SIMULATIONS AND EXPERIMENTS

A. Experimental setup

For the purpose of the present paper, we experimentally recreate the simulated system of Fig. 1, as shown and briefly captioned in Fig. 3 (adapted from [50]). In addition to the components of Fig. 1, the setup also includes a quarter wave plate (QWP) and a Glan-Thompson polarizer (GTP) after the lens L_2 in order to make Stokes measurements [62] on the final output beam. The various parameters considered for the simulation and the experiment are refractive indices $n_1 = 1$, $n_2 = 1.52$; power and free-space wavelength of the laser, $P_w = 1$ mW, $\lambda = 632.8$ nm; half width of the input beam, $w_0 = 0.6$ mm; focal lengths of the lenses, $\mathcal{F}_1 = -5$ cm, $\mathcal{F}_2 = 12.5$ cm; propagation distances $O_I O_S = 5$ cm, $O_S O_R = 2.5$ cm.
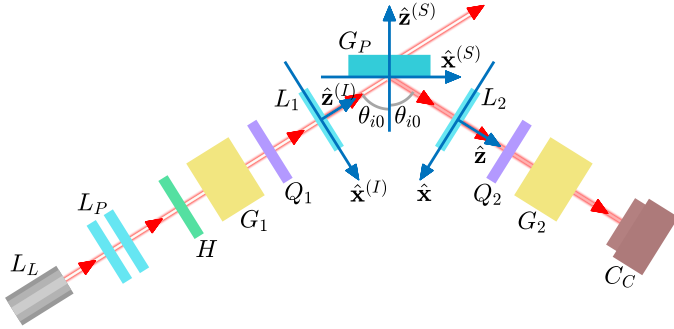
FIG. 3. The experimental setup, comprising a He-Ne laser L_L, a collimating lens-pair L_P, a half wave plate H, Glan-Thompson polarizers G_1 and G_2, quarter wave plates Q_1 and Q_2, diverging and collimating lenses L_1 and L_2, a glass plate G_P whose surface is used as the dielectric interface, and a CCD camera C_C which represents the screen of observation S_R (Fig. 1) (adapted from [50]).
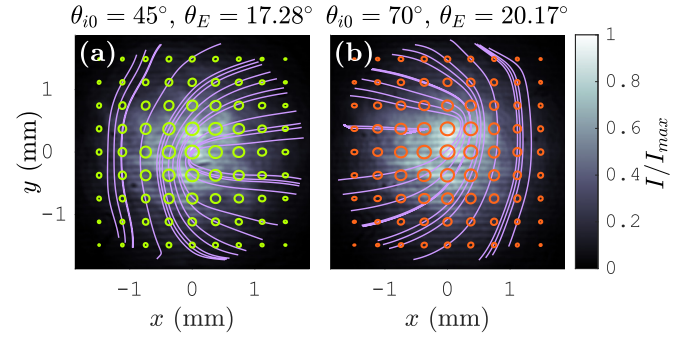

FIG. 5. Experimentally obtained field profiles [64] corresponding to the simulated profiles of Figs. 4(a) and 4(c), showing a reasonable match between the simulations and experiments [experimental verification of the profile of Fig. 4(b) can be found in Ref. [50]].

B. Simulated and experimental examples

We have computationally generated field profiles for various θ_{i0} values with the condition of Eq. (5a) applied, including the $\theta_{i0} = \theta_B$ case, and have obtained the expected polarization singularities. Simulated examples of polarization-singular field profiles for $\theta_{i0} = 45°$, $56.66°$ (θ_B), and $70°$ are shown in Fig. 4 [63]. Corresponding to these θ_{i0} values, the θ_{ES} values are obtained from Eq. (5a) as $\theta_{ES} \approx \pm17.28°, 0°$ and $\pm20.17°$. The profiles of Fig. 4 are obtained by considering only the positive parameter values $\theta_E = +|\theta_{ES}|$ and $\Phi_E = +\pi/2$.

The profile for the $\theta_{i0} = \theta_B$ case [Fig. 4(b)] matches well with the result of our earlier work [50], showing the formation of a V-point singularity [47] with a node pattern of the streamlines [28]. The profiles of Figs. 4(a) and 4(c) show examples of a $\theta_{i0} < \theta_B$ case and a $\theta_{i0} > \theta_B$ case, which contain a central $\hat{\boldsymbol{\sigma}}^-$ polarization and a central $\hat{\boldsymbol{\sigma}}^+$ polarization respectively—i.e., C-point singularities—associated with opposite lemon patterns of the streamlines [28]. In the profile of Fig. 4(a), the $\hat{\boldsymbol{\sigma}}^-$ polarization significantly dominates over the

$\hat{\boldsymbol{\sigma}}^+$ polarization, whereas the opposite happens in the profile of Fig. 4(c). Because of the massive dominance of one spin polarization over the other, the elliptical natures of the polarization ellipses are not visually recognizable in these figures, but are understandable only by observing the streamlines. The central points with abrupt turns of the streamlines (due to indeterminate ellipse orientation) are the pure spin polarization points, i.e., the C-point singularities. On the other hand, in the profile of Fig. 4(b), both $\hat{\boldsymbol{\sigma}}^{\pm}$ polarizations have equal contributions [50], thus squeezing the polarization ellipses to linear shapes [63]. The central point, where the handedness and orientation of the polarization ellipse are both indeterminate (because the field is zero), is a V-point singularity [47].

The profiles for the negative parameter values $\theta_E = -|\theta_{ES}|$ and $\Phi_E = -\pi/2$ are straightforward to obtain and are not shown here. We have observed in the simulation that, by transforming either $\theta_E \to -\theta_E$ or $\Phi_E \to -\Phi_E$, the handedness of the central spin polarization can be flipped, whereas changing both signs keeps the handedness unchanged.
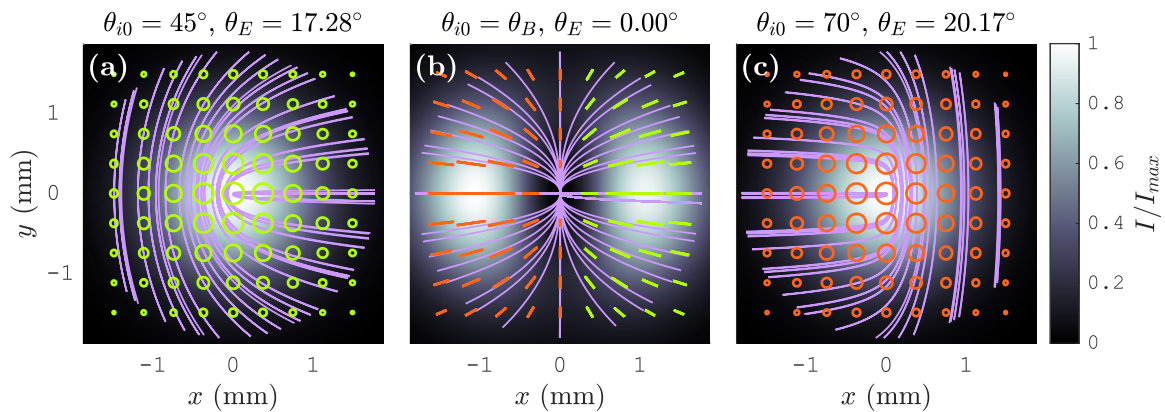

FIG. 4. Simulated polarization-singular field profiles [63] for (a) $\theta_{i0} = 45°$ and $\theta_E \approx 17.28°$ (obtained $I_{max} \approx 4.83$ W/m^2); (b) $\theta_{i0} = \theta_B \approx 56.66°$ and $\theta_E = 0°$ (obtained $I_{max} \approx 2.93$ mW/m^2); and (c) $\theta_{i0} = 70°$ and $\theta_E \approx 20.17°$ (obtained $I_{max} \approx 20.73$ W/m^2). For each profile we have chosen $\Phi_E = +\pi/2$. Color codes: The light green ellipses in (a) represent left-elliptical (i.e., $\hat{\boldsymbol{\sigma}}^-$-dominant) polarizations (LEP); the dark orange ellipses in (c) represent right-elliptical (i.e., $\hat{\boldsymbol{\sigma}}^+$-dominant) polarizations (REP); the light green and dark orange line segments in (b), respectively, represent LEP-transformed-to-linear and REP-transformed-to-linear polarizations [63]. The purple streamlines represent the major axis orientation patterns of the polarization ellipses.

Figure 5 shows the experimentally generated field profiles corresponding to the simulated profiles of Figs. 4(a) and 4(c), respectively (the $\theta_{i0} < \theta_B$ and $\theta_{i0} > \theta_B$ cases; the experimental verification for $\theta_{i0} = \theta_B$ [Fig. 4(b)] can be found in Ref. [50]). We have obtained these experimental field profiles by analyzing the results of Stokes measurements [62,64] performed on the output beam [Fig. 3]. The experimental profiles match the corresponding simulated profiles well, thus verifying the formation of the expected polarization singularities.

In the light of the above analysis, it is evident that the formation of an isolated C-point singularity in Figs. 4(c) and 6(c) of Ref. [50] is simply an example of an off-Brewster incidence case of the present generalized formalism—which is another remarkable result here.

C. Phase singularity of a spin-component field

Since a C-singularity point is a point of an isolated circular polarization surrounded by noncircular polarizations, it is implied that the contribution of the orthogonal circular polarization is precisely zero at that point and nonzero at the surrounding points. This indicates that, at the C-singularity point, the orthogonal circular polarization contains a phase singularity (vortex). This is exactly the way a phase singularity and a polarization singularity are interrelated—a circularly polarized field with a constant (or almost constant) phase profile and the orthogonal-circularly polarized field with a phase singularity superpose to generate a C-point polarization singularity [28,45,50].

To examine the phase singularity characteristics in the present work, we consider the beam-field profile for $(\theta_{i0}, \theta_E, \Phi_E) = (45°, 17.28°, \pi/2)$ [Figs. 4(a) and 5(a)], which contains a central C-singularity with a $\hat{\sigma}^-$ spin polarization. This implies that the $\hat{\sigma}^+$-polarized component field must contain a phase singularity at the beam center in this case.

To isolate the $\hat{\sigma}^+$ contribution to the total field, we first propagate the output beam through a QWP, oriented to introduce an additional $+\pi/2$ phase to the $\hat{x}$ component. This transforms the $\hat{\sigma}^\pm$ polarizations to $\hat{d}^\pm = (\hat{x} \pm \hat{y})/\sqrt{2}$ polarizations. Then, by passing the QWP-output beam through a GTP, with its transmission axis oriented along $\hat{d}^+$, a controlled $\hat{d}^+$-polarized output beam is obtained—whose intensity and phase profiles are equivalent to those of the original $\hat{\sigma}^+$ component field. The properties of this controlled output beam are then easily examined to reveal the properties of the original $\hat{\sigma}^+$-polarized field.

The simulated phase profile of the $\hat{\sigma}^+$ component field is shown in Fig. 6(a), which reveals the existence of an $l = -1$ phase vortex at the beam center. We experimentally verify this phase characteristic by obtaining a single-slit diffraction pattern. We pass the controlled output beam through a single vertical slit of width 0.4 mm, placed along $x = 0$. The obtained far-field diffraction pattern [Fig. 6(b)] is the characteristic single-slit diffraction pattern of an $l = -1$ phase vortex [65]. This observation verifies the existence of the phase vortex in the controlled output beam.

Thus, by using the methods of the present subsection, the phase vortex characteristics of the polarization-singular output beam field are analyzed and experimentally verified. This
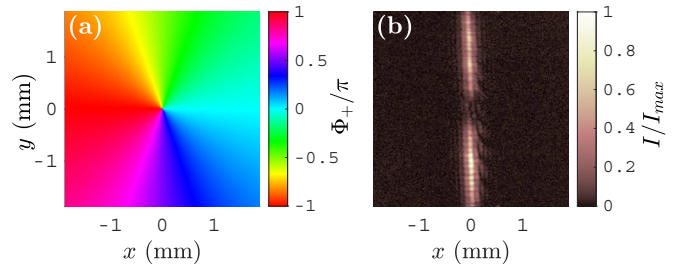

FIG. 6. (a) Phase profile of the $\hat{\sigma}^+$-polarized component field corresponding to the polarization-singular total beam field of Fig. 4(a), exhibiting an $l = -1$ phase vortex. (b) Single-slit diffraction pattern of the $\hat{\sigma}^+$-converted-to-$\hat{d}^+$ controlled output beam, showing the characteristic fringe dislocation due to an $l = -1$ phase vortex.

vortex nature, and thus an orbital angular momentum (OAM), clearly manifests itself due to the inhomogeneous nature of the reflection process, even when the initial input beam contains only spin angular momentum. This indicates some amount of spin-to-orbital angular momentum conversion—a manifestation of SOI—happening in the system due to the reflection process.

D. Variation of θ_E for a fixed θ_{i0}

Until now, for a fixed θ_{i0} value, we have used $\theta_E = \theta_{ES}$ determined by Eq. (5a) to obtain the intended singularity at $x = 0$. In this subsection, we vary θ_E around this central θ_{ES} value for the fixed θ_{i0} to observe the shift of the singularity from the beam center, following the general condition of Eq. (4).

We choose the fixed value $\theta_{i0} = 45°$ as in Figs. 4(a) and 6. We then choose displaced θ_E values 17.08° and 17.48°, which are $\pm 0.2°$ shifted from the previously used value 17.28° that produces the central singularity [Figs. 4(a) and 6(a)]. The simulated polarization-singular total beam fields for $\theta_E \approx$ 17.08°, 17.28°, and 17.48° are shown in Figs. 7(a), 7(b), and 7(c), respectively, which show the singularity positions in the $x < 0$ region, at $x = 0$, and in the $x > 0$ region. The phase-singular $\hat{\sigma}^+$ component field also undergoes corresponding transformations—as understood from its casewise simulated intensity profiles of Figs. 7(d), 7(e), and 7(f)—because the polarization singularity of the total field and the phase singularity of the $\hat{\sigma}^+$ field appear at the same point. The casewise experimentally observed $\hat{\sigma}^+$-converted-to-$\hat{d}^+$ controlled output intensity profiles are shown in Figs. 7(g), 7(h), and 7(i), respectively, which match the corresponding simulated $\hat{\sigma}^+$ intensity profiles [Figs. 7(d), 7(e), and 7(f)] well. Thus, the condition of Eq. (4) is verified from a general perspective in terms of central as well as off-central singularity formations.

One can easily visualize that, as the θ_E value is gradually taken from 17.08° to 17.48° through 17.28°, the singularity position x_S moves from the $x < 0$ to the $x > 0$ region through $x = 0$. Correspondingly, the Fig. 7(a) [or Fig. 7(d) or Fig. 7(g)] profile gradually transforms to the Fig. 7(c) [or Fig. 7(f) or Fig. 7(i)] profile through the intermediate profile of Fig. 7(b) [or Fig. 7(e) or Fig. 7(h)]. This phenomenon reveals a significant transitional dynamics of the polarization and phase singularities that are demonstrated in the present paper [63].
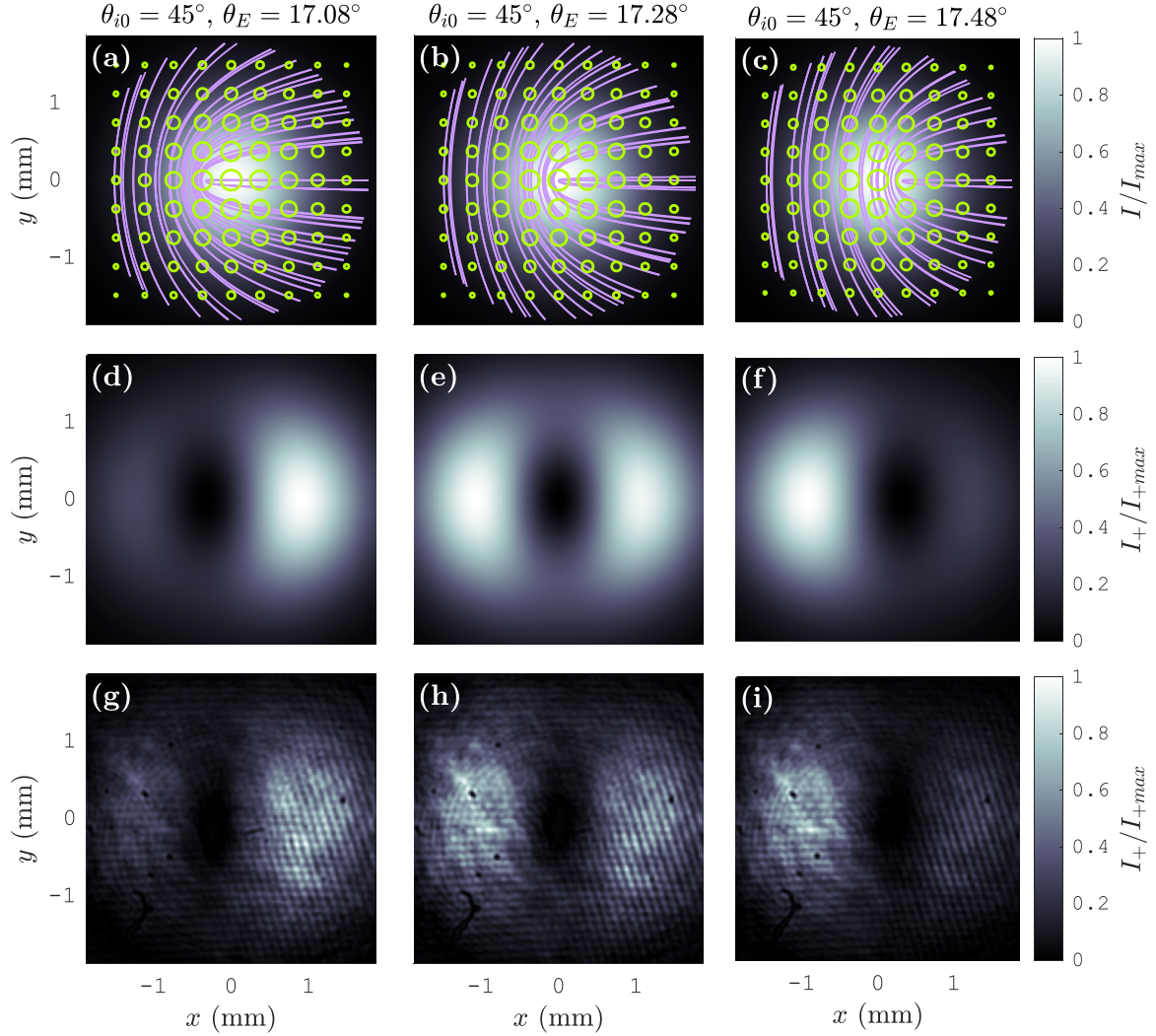
FIG. 7. (a, b, c) Simulated polarization-singular total field profiles for $\theta_{i0} = 45°$ and $\theta_E \approx 17.08°$, $17.28°$, $17.48°$, showing the singularity positions in the $x < 0$ region, at $x = 0$, and in the $x > 0$ region respectively. The obtained I_{max} values are respectively 4.78 W/m^2, 4.83 W/m^2, and 4.88 W/m^2. (d, e, f) Simulated intensity (I_+) profiles of the phase-singular $\hat{\sigma}^+$ component field corresponding to (a), (b), and (c). The obtained I_{+max} values are respectively 1.25 mW/m^2, 0.74 mW/m^2, and 1.29 mW/m^2 [63]. (g, h, i) Corresponding experimentally observed intensity profiles of the $\hat{\sigma}^+$-converted-to-$\hat{d}^+$ controlled output field.

V. BEAM SHIFTS, SPIN SHIFTS, AND A GENERALIZED PERSPECTIVE

The central content of the present paper, as demonstrated above, is the identification and control of generic optical singularity characteristics of a reflected paraxial beam field; and we have used a Fresnel-coefficient-based calculation only at the central plane of incidence to identify these singularities. However, we emphasize that these singularity characteristics are a subset of a much larger set of phenomena exhibited by the concerned inhomogeneously polarized reflected beam field. Following our work of Ref. [51], we have obtained the simulated fields via the generalized reflection and transmission coefficient matrix formalism, due to which the complete and exact vectorial information on the reflected beam field is available. As discussed in Ref. [51], the availability of the complete field information serves as the foundation for determining all special beam-field properties such as GH and IF shifts, longitudinal and transverse spin shifts including the

spin-Hall effect of light (SHEL) [16,19], and the underlying geometric phase properties of the field. From this perspective, we assert that all these special beam-field phenomena and the optical singularity generation discussed in the present paper are interrelated, since they are manifestations of different properties of the same inhomogeneously polarized field. In this section we demonstrate the GH, IF, and spin shift phenomena of the reflected field under the considered context of singularity formation in order to show the interdependence of these seemingly unrelated effects. Then we identify possible ways to achieve further generalization of our work from the perspective of availability of the complete field information.

A. GH and IF shifts

The GH shift of the beam is the longitudinal (i.e., along the x axis) shift of the beam centroid from the central-ray point O (Fig. 1). As discussed in Ref. [51], the reflected fields corresponding to the individual $\mathcal{E}_{0x}^{(I)} \hat{x}^{(I)}$ and $\mathcal{E}_{0y}^{(I)} \hat{y}^{(I)}$ input
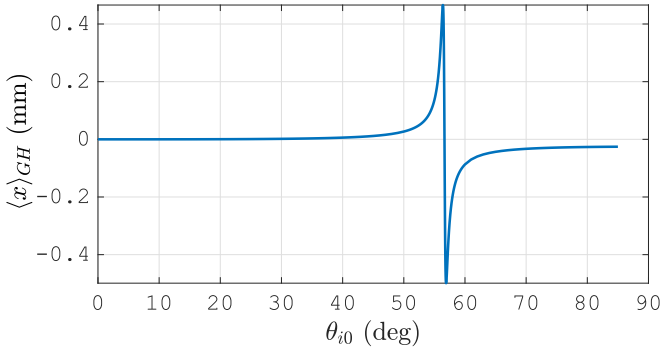
FIG. 8. Variation of the GH shift $\langle x \rangle_{GH}$ of the total output beam field as a function of θ_{i0}, considering the associated θ_E variation as $\theta_E = \theta_{ES}$ [Eq. (5a), Fig. 2] for singularity generation at the beam center. The plot shows large GH shifts (comparable to the half-beam-width w_R) for near-Brewster incidence. A zero centroid shift is observed not exactly for the Brewster angle, but for a nearby angle $\theta_{i0} \approx 56.65°$, due to the slight asymmetry of the Brewster-reflected intensity profile [Fig. 4(b)] with respect to the y axis.

fields [Eq. (1a)] experience their own GH shifts which vary with θ_{i0}—and these individual GH shifts contribute to the GH shift of the total beam field $\mathcal{E}$ [Eq. (2a)]. The contribution of the $\mathcal{E}_{0x}^{(I)} \hat{\mathbf{x}}^{(I)}$ and $\mathcal{E}_{0y}^{(I)} \hat{\mathbf{y}}^{(I)}$ fields in the total input is determined by θ_E [Eq. (1b)], which, in the present context of singularity generation, is set to θ_{ES} determined by Eq. (5a). This results in a unique variation of GH shift of the total beam field as a function of θ_{i0}, with the readjustment of θ_E for every θ_{i0} value taken into account (Fig. 8) [63]. This variation also reveals an unobvious fact that the polarization singularities in the field profiles of Fig. 4 are not in general formed at the beam-centroid positions because the condition of Eq. (5a) ensures the formation of the singularities at the central point O, whereas the beam-centroid positions are GH-shifted according to the variation shown in Fig. 8. The variation also shows particularly large (comparable to the effective half-beam-width w_R [Eq. (2c)]) GH shifts for near-Brewster angles of incidence, which is consistent with the effects described by Chan and Tamir [7].

Unlike the GH shift, which does not depend on the phase Φ_E [Eq. (1a)], the IF shift depends on all the three parameters $(\theta_{i0}, \theta_E, \Phi_E)$. As explained graphically in Ref. [50], the output fields corresponding to the $\mathcal{E}_{0x}^{(I)} \hat{\mathbf{x}}^{(I)}$ and $\mathcal{E}_{0y}^{(I)} \hat{\mathbf{y}}^{(I)}$ inputs, for a general Φ_E, superpose to create an asymmetry in the total beam field with respect to the x axis. Because of this asymmetry, the centroid of the total beam field undergoes a transverse (i.e., along the y axis) shift, which is the IF shift of the total beam field. However, we have verified that the assignment $\Phi_E = \Phi_{ES} = \pm \pi/2$ [Eq. (4)] eliminates this asymmetry in the total intensity profile in the present case. The y shift of the total beam centroid is thus reduced to zero, resulting in a zero IF shift in the presently considered case.

B. Spin shifts and spin-Hall effect

In terms of the presently available complete field information, the spin shifts are interpreted straightforwardly as the centroid shifts of the $\hat{\boldsymbol{\sigma}}^{\pm}$ field intensity profiles. These centroid shifts also depend on the three parameters $(\theta_{i0}, \theta_E, \Phi_E)$. For
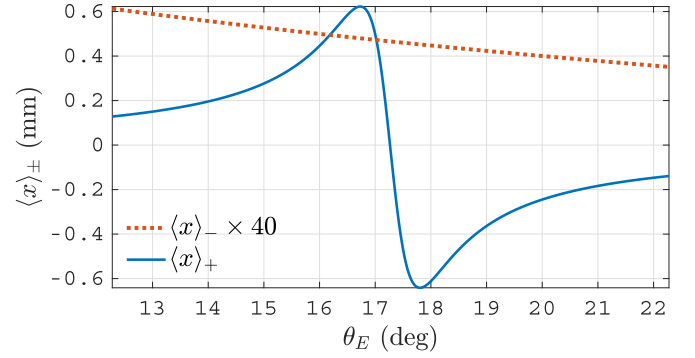

FIG. 9. Variations of the longitudinal centroid shifts $\langle x \rangle_{\pm}$ of the output $\hat{\boldsymbol{\sigma}}^{\pm}$ intensity profiles as functions of θ_E around the central θ_{ES} value 17.28° for $\theta_{i0} = 45°$ [Eq. (5a)]. The plot shows large $\hat{\boldsymbol{\sigma}}^{+}$ spin shifts (comparable to the half-beam-width w_R) on both sides of $\theta_E = 17.28°$. A zero centroid shift is observed for $\theta_E = 17.27°$ but not for 17.28°, due to the slight asymmetry of the $\hat{\boldsymbol{\sigma}}^{+}$ intensity profile [Fig. 7(e)] with respect to the y axis. The $\hat{\boldsymbol{\sigma}}^{-}$ spin shift has much smaller values as compared to the $\hat{\boldsymbol{\sigma}}^{+}$ spin shift; and hence it is represented here by multiplying with 40.

the present demonstration we consider the fixed $\theta_{i0} = 45°$ case of Sec. IV D (Fig. 7) and show the centroid-shift characteristics by varying θ_E around the central θ_{ES} value 17.28°.

As mentioned in Fig. 7, the maximum intensity of the total field for $(\theta_{i0}, \theta_E) = (45°, 17.28°)$ is $I_{\max} = 4.83$ W/m^2, whereas that of the $\hat{\boldsymbol{\sigma}}^{+}$ field for the same parameter values is $I_{+\max} = 0.74$ mW/m^2. The dominant $\hat{\boldsymbol{\sigma}}^{-}$ field thus hugely outweighs the remnant $\hat{\boldsymbol{\sigma}}^{+}$ field, because of which, the $\hat{\boldsymbol{\sigma}}^{-}$ field characteristics are nearly identical to the total beam-field characteristics. In particular, the longitudinal and transverse shifts of the $\hat{\boldsymbol{\sigma}}^{-}$ intensity centroid are respectively nearly identical to the GH and IF shifts of the total field—a special behavior of the presently considered polarization-singular field.

The variation of the longitudinal shift of the $\hat{\boldsymbol{\sigma}}^{-}$ intensity centroid in a θ_E range $\pm 5°$ around the central value 17.28° is shown in Fig. 9. As θ_E is varied, the contribution of the $\mathcal{E}_{0x}^{(I)} \hat{\mathbf{x}}^{(I)}$ and $\mathcal{E}_{0y}^{(I)} \hat{\mathbf{y}}^{(I)}$ fields in the total input varies [Eq. (1b)]—resulting in a variation of the GH shift of the total field and a consequent variation of the longitudinal $\hat{\boldsymbol{\sigma}}^{-}$ spin shift. However, due to the consideration of $\Phi_E = \pm \pi/2$, we obtain a $\hat{\boldsymbol{\sigma}}^{-}$ intensity profile which is symmetric with respect to the x axis. This results in a zero transverse shift of the $\hat{\boldsymbol{\sigma}}^{-}$ intensity centroid, which is consistent with the zero IF shift of the total field.

The transverse shift of the $\hat{\boldsymbol{\sigma}}^{+}$ intensity centroid is zero likewise. However, due to the transitional dynamics of the phase singularity of the $\hat{\boldsymbol{\sigma}}^{+}$ field [Figs. 7(d), 7(e), and 7(f)], a significant variation of the longitudinal (x) position of the $\hat{\boldsymbol{\sigma}}^{+}$ intensity centroid is observed. As seen in Fig. 7, as the phase singularity moves from the $x < 0$ region to the $x > 0$ region, the centroid of the I_+ profile shifts drastically along the opposite direction—resulting in enormous longitudinal centroid shifts on both sides of $x = 0$, comparable to the effective half-width w_R [Eq. (2c)] of the total field [63]. The variation of the longitudinal centroid shift of the I_+ intensity profile is shown in Fig. 9 for a θ_E range $\pm 5°$ around the central value

17.28°—where the unique nature of this longitudinal $\hat{\boldsymbol{\sigma}}^{+}$ spin shift is clearly observed.

Finally, since the longitudinal shifts of the $\hat{\boldsymbol{\sigma}}^{\pm}$ intensity centroids are different, a well-defined longitudinal spin separation is obtained in the present case. However, since the transverse shifts of these centroids are both zero, no corresponding transverse separation is obtained. The spin-Hall effect of light, which signifies the transverse spin separation in the beam field, is thus zero in the presently considered polarization-singular fields. We have verified in the simulation that, if we move away from the singularity formation condition of Eq. (4) by taking $\Phi_E \neq \pm\pi/2$, we obtain $\hat{\boldsymbol{\sigma}}^{\pm}$ intensity profiles which are asymmetric with respect to the x axis. This results in nonzero transverse shifts of the $\hat{\boldsymbol{\sigma}}^{\pm}$ intensity centroids. Except for two special cases $\Phi_E = 0, \pi$, these centroid shifts are unequal, resulting in a transverse separation between the centroids. Nonzero spin-Hall shifts are thus achieved in such cases by perturbing the singularity formation.

C. Further generalization and future directions

In Sec. IV C we have interpreted the manifestation of SOI by identifying the partial conversion from spin to orbital angular momentum. Due to the availability of the complete field information, the next step in the present formalism would be to mathematically characterize this phenomenon by determining the exact spin and orbital contributions to the total angular momentum of the field—which can be achieved by following the methods of Allen *et al.* [59], Berry [60], and Barnett [61]. The relevant detailed mathematical analysis is outside the scope of the present paper. But this anticipation further strengthens our assertion that all the unique beam-field phenomena are manifestations of different characteristics of the same inhomogeneously polarized beam field—and with the complete information on the beam field, all these phenomena and their interrelations can be seamlessly explained under the same formalism. We strongly anticipate that the complete mathematical characterization of SOI would be particularly significant and fundamentally interesting in the context of the generic optical singular fields considered in the present paper.

Even though we have demonstrated our central context of singularity generation by considering the interrelation of phase and polarization singularities, we emphasize that a phase singularity can exist without an associated polarization singularity. For example, if the optical system is configured to give a certain elliptical polarization $\hat{\mathbf{e}}_1$ in an ideal reflected plane-wave field, the reflected paraxial beam field attains the polarization $\hat{\mathbf{e}}_1$ only at the beam center, surrounded by other elliptical polarizations. Clearly, this inhomogeneously polarized beam field can be interpreted as a superposition of (1) the dominant $\hat{\mathbf{e}}_1$-polarized field with a constant or almost-constant phase profile and (2) the remnant orthogonally polarized (e.g., $\hat{\mathbf{e}}_2$, orthogonal to $\hat{\mathbf{e}}_1$ on the Poincaré sphere) field with a phase singularity. Thus, a phase-singular $\hat{\mathbf{e}}_2$-polarized field is obtained, even though the total field does not contain a polarization singularity. Interpreted from an experimental perspective, one can exactly cancel the elliptical polarization at a specific point in the beam field by using an appropriately configured QWP-GTP combination. This operation removes the contribution of that specific elliptical polarization from the entire beam field. The controlled output thus obtained contains contribution from only the orthogonal elliptical polarization, with a phase singularity at the point where the original field has been exactly canceled.

Clearly, any general inhomogeneously polarized paraxial beam field can be expressed in this way as a dominant-remnant field superposition. Since the beam shifts, spin shifts, and SOI phenomena are simply different manifestations of the fundamental inhomogeneity of the beam field, the above discussion indicates the significant possibility that all such special phenomena arising in a complex reflected (or transmitted) beam field must be strongly correlatable to the superposition characteristics of a dominant plane-wave or near-plane-wave field and a remnant orthogonally polarized phase-singular field. This possible perspective is a fundamentally appealing generalized view of our present formalism, which can potentially lead to a different direction for future exploration.

Finally, we emphasize that our method of generic singularity formation can find potential application in experimental measurement of refractive indices of dielectric materials. As seen in Fig. 7, the singularity position in the beam field is very sensitive to θ_E. The central θ_{ES} value, as determined by Eq. (5a), depends on θ_{i0} as well as on the refractive indices n_1 and n_2. Experimentally determined (θ_{i0}, θ_E) pairs that create the central singularity as in Fig. 7(h) thus contain information on n_1 and n_2 with significant accuracy. This measurement can thus be utilized to determine an unknown refractive index n_2 (while using $n_1 = 1$ for air)—a potential technique whose efficiency and accuracy is to be explored in the future.

VI. CONCLUSION

In the present paper, we have identified a generalized condition on the input polarization that can generate a C-point polarization singularity in a reflected paraxial beam field for any central angle of incidence. Associated with this polarization singularity, we have characterized the phase singularity of the constituent field whose polarization is orthogonal to the central circular polarization. Singularity generation due to Brewster reflection [48–50] is seamlessly understood as a special case of the present formalism. We have demonstrated these polarization and phase singularities via simulated profiles and have verified them experimentally. Finally, we have demonstrated the dynamics of the singularities due to controlled variation of the input polarization. The result that phase and polarization singularities can be generated by a single reflection of a paraxial beam at a plane isotropic dielectric interface—due to any general central angle of incidence—is the central feature of our formalism.

Even though we have derived the singularity generation condition by using a Fresnel-coefficient-based calculation only at the central plane of incidence, we have demonstrated the simulated field profiles by obtaining exact output field information via our generalized reflection and transmission coefficient matrix formalism. By virtue of this availability of complete field information, we have explored the unique natures of the GH, IF, and spin shifts of the optical-singular beam fields. We have proposed that the SOI phenomena of the presently considered fields can be completely

characterized mathematically by using the available exact field information, which would be fundamentally significant to explore especially due to the involvement of optical singularity formations. Finally, by explaining the generation of a phase-singular field independent of a polarization singularity, we have demonstrated a special decomposition of an inhomogeneously polarized field as a superposition of a dominant plane-wave or near-plane-wave field and a remnant orthogonally polarized phase-singular field. The special beam-field phenomena studied in the literature and the optical-singular phenomena discussed in the present paper are all interrelated, as they are manifestations of the same fundamental polarization inhomogeneity of the beam field. While some of these interrelations are explored in the present paper, we anticipate

that further detailed exploration in this direction—especially a complete mathematical characterization of SOI phenomena in the present singularity formation context—would provide a very rich and significant understanding of the fundamental polarization-inhomogeneity characteristics of a reflected paraxial beam field. Additionally, our singularity formation method can have potential application in experimental characterization of dielectric media, especially in measurements of unknown refractive indices.

[1] M. Born and E. Wolf, *Principles of Optics*, 7th ed. (Cambridge University Press, Cambridge, 1999).

[2] V. F. Goos and H. Hänchen, Ann. Phys. **436**, 333 (1947).

[3] K. Artmann, Ann. Phys. **437**, 87 (1948).

[4] J. W. Ra, H. L. Bertoni, and L. B. Felsen, SIAM J. Appl. Math. **24**, 396 (1973).

[5] Y. M. Antar and W. M. Boerner, Can. J. Phys. **52**, 962 (1974).

[6] M. McGuirk and C. K. Carniglia, J. Opt. Soc. Am. **67**, 103 (1977).

[7] C. C. Chan and C. Tamir, Opt. Lett. **10**, 378 (1985).

[8] M. A. Porras, Opt. Commun. **131**, 13 (1996).

[9] A. Aiello and J. P. Woerdman, arXiv:0903.3730 (2009).

[10] F. I. Fedorov, Dokl. Akad. Nauk SSSR **105**, 465 (1955), English translation available at http://master.basnet.by/congress2011/symposium/spbi.pdf.

[11] H. Schilling, Ann. Phys. **471**, 122 (1965).

[12] C. Imbert, Phys. Rev. D **5**, 787 (1972).

[13] M. A. Player, J. Phys. A: Math. Gen. **20**, 3667 (1987).

[14] V. G. Fedoseyev, J. Phys. A: Math. Gen. **21**, 2045 (1988).

[15] V. S. Liberman and B. Y. Zel'dovich, Phys. Rev. A **46**, 5199 (1992).

[16] M. Onoda, S. Murakami, and N. Nagaosa, Phys. Rev. Lett. **93**, 083901 (2004).

[17] K. Y. Bliokh and Y. P. Bliokh, Phys. Rev. Lett. **96**, 073903 (2006).

[18] K. Y. Bliokh and Y. P. Bliokh, Phys. Rev. E **75**, 066609 (2007).

[19] O. Hosten and P. Kwiat, Science **319**, 787 (2008).

[20] A. Aiello and J. P. Woerdman, arXiv:0710.1643 (2007).

[21] A. Aiello and J. P. Woerdman, Opt. Lett. **33**, 1437 (2008).

[22] M. Merano, A. Aiello, M. P. van Exter, and J. P. Woerdman, Nat. Photon **3**, 337 (2009).

[23] A. Aiello, M. Merano, and J. P. Woerdman, Phys. Rev. A **80**, 061801(R) (2009).

[24] Y. Qin, Y. Li, X. Feng, Y.-F. Xiao, H. Yang, and Q. Gong, Opt. Express **19**, 9636 (2011).

[25] K. Y. Bliokh and A. Aiello, J. Opt. **15**, 014001 (2013).

[26] J. B. Götte, W. Löffler, and M. R. Dennis, Phys. Rev. Lett. **112**, 233901 (2014).

[27] L. Xie, X. Zhou, X. Qiu, L. Luo, X. Liu, Z. Li, Y. He, J. Du, Z. Zhang, and D. Wang, Opt. Express **26**, 22934 (2018).

[28] G. J. Gbur, *Singular Optics* (CRC Press, Boca Raton, FL, 2017).

[29] J. F. Nye and M. V. Berry, Proc. R. Soc. London A **336**, 165 (1974).

[30] R. Bhandari, Phys. Rep. **281**, 1 (1997).

[31] M. S. Soskin, V. N. Gorshkov, M. V. Vasnetsov, J. T. Malos, and N. R. Heckenberg, Phys. Rev. A **56**, 4064 (1997).

[32] M. Padgett and A. Allen, Contemp. Phys. **41**, 275 (2000).

[33] M. S. Soskin and M. V. Vasnetsov, Prog. Opt. **42**, 219 (2001).

[34] M. R. Dennis, K. O'Holleran, and M. J. Padgett, Prog. Opt. **53**, 293 (2009).

[35] K. Y. Bliokh and F. Nori, Phys. Rep. **592**, 1 (2015).

[36] M. V. Berry and J. H. Hannay, J. Phys. A: Math. Gen. **10**, 1809 (1977).

[37] J. F. Nye, Proc. R. Soc. London A **387**, 105 (1983).

[38] J. F. Nye, Proc. R. Soc. London A **389**, 279 (1983).

[39] J. V. Hajnal, Proc. R. Soc. London A **414**, 433 (1987).

[40] J. V. Hajnal, Proc. R. Soc. London A **414**, 447 (1987).

[41] J. F. Nye and J. V. Hajnal, Proc. R. Soc. London A **409**, 21 (1987).

[42] T. Delmarcelle and L. Hesselink, in *Proc. Visualization '94* (IEEE, 1994), pp. 140–147.

[43] M. R. Dennis, Opt. Commun. **213**, 201 (2002).

[44] M. R. Dennis, Opt. Lett. **33**, 2572 (2008).

[45] N. K. Viswanathan, V. Kumar, and G. M. Philip, J. Opt. **15**, 044027 (2013).

[46] Y. V. Jayasurya, V. V. G. K. Inavalli, and N. K. Viswanathan, Appl. Opt. **50**, E131 (2011).

[47] Ruchi, S. K. Pal, and P. Senthilkumaran, Opt. Express **25**, 19326 (2017).

[48] R. Barczyk, S. Nechayev, M. A. Butt, G. Leuchs, and P. Banzer, Phys. Rev. A **99**, 063820 (2019).

[49] A. Debnath and N. K. Viswanathan, in *Conference on Lasers and Electro-Optics* (Optical Society of America, Washington, DC, 2020), p. JTh2E.1.

[50] A. Debnath and N. K. Viswanathan, Phys. Rev. A **103**, 013510 (2021).

[51] A. Debnath and N. K. Viswanathan, J. Opt. Soc. Am. A **37**, 1971 (2020).

[52] S. Pancharatnam, Proc. Ind. Acad. Sci. A **44**, 247 (1956).

[53] M. V. Berry, Proc. R. Soc. Lond. A **392**, 45 (1984).

[54] M. V. Berry, J. Mod. Opt. **34**, 1401 (1987).

[55] A. Shapere and F. Wilczek, *Geometric Phases in Physics* (World Scientific, Singapore, 1989).

[56] K. Y. Bliokh, Y. Gorodetski, V. Kleiner, and E. Hasman, Phys. Rev. Lett. **101**, 030404 (2008).

[57] K. Y. Bliokh, J. Opt. A: Pure Appl. Opt. **11**, 094009 (2009).

[58] K. Y. Bliokh, M. A. Alonso, E. A. Ostrovskaya, and A. Aiello, Phys. Rev. A **82**, 063825 (2010).

[59] L. Allen, M. W. Beijersbergen, R. J. C. Spreeuw, and J. P. Woerdman, Phys. Rev. A **45**, 8185 (1992).

[60] M. V. Berry, in *Proc. SPIE*, vol. 3487 (SPIE, 1998), pp. 6–11.

[61] S. M. Barnett, J. Opt. B **4**, S7 (2002).

[62] D. H. Goldstein, *Polarized Light*, 3rd ed. (CRC Press, Boca Raton, FL, 2011).

[63] See Supplemental Material at http://link.aps.org/supplemental/10.1103/PhysRevA.106.013522 for (1) an animated variation of the total field profile due to variation of θ_{i0}, considering $\theta_E = +|\theta_{ES}|$ and $\Phi_E = +\pi/2$ for singularity formation; and (2) an animated variation of the total field and the $\hat{\sigma}^+$ field intensity profile due to variation of θ_E around the central value $\theta_{ES} = 17.28°$ for $\theta_{i0} = 45°$ and $\Phi_E = +\pi/2$.

[64] In the experiment, the beam-profile images are captured by the CCD camera for the different Stokes measurement configurations. This implies the collection of the Stokes measurement data at each pixel of the camera. Subsequently the polarization information is obtained at each pixel by using these data. An experimental field profile, such as the ones plotted in Fig. 5, can thus be understood as a collection of the intensity and polarization information at all the pixels of the CCD camera.

[65] D. P. Ghai, P. Senthilkumaran, and R. S. Sirohi, Opt. Laser Eng. **47**, 123 (2009).